Polar Chirality in BiFeO₃ Emerging from A Peculiar Domain Wall Sequence

Stéphane Fusil,* Jean-Yves Chauleau, Xiaoyan Li, Johanna Fischer, Pauline Dufour, Cyril Léveillé, Cécile Carrétéro, Nicolas Jaouen, Michel Viret, Alexandre Gloter, and Vincent Garcia*

Topological states are currently gathering intensive investigation in condensed matter physics due to their potential as configurable electronic devices for the future era coined "topotronics." Beyond numerous breakthroughs in magnetism over the past decade, a new paradigm is emerging with the proposal of topologically protected objects in ferroelectric materials. Recently, ferroelectric skyrmions and vortices are observed in PbTiO₃/SrTiO₃ superlattices, opening the path toward ultra-small topological objects with low-power electric-field control. Here, the observation of chiral polar windings in a single epitaxial thin film, triggered by its self-organized stripe domain pattern arrangement, is reported. Combining resonant elastic X-ray scattering and scanning transmission electron microscopy, signatures of polar chirality in epitaxial BiFeO₃ thin films corroborated with a complex ferroelectric domain wall structure are shown. The net chirality suggests that domain walls induce a polar rotation through a small path alternating with an unexpected long path at every second domain wall. In addition, scanning probe microscopy reveals singularities associated to this peculiar domain wall structure. These results bring new insights into the unexpected complexity of standard striped-domain BiFeO₃ thin films and open questions as for the driving force of this polar chirality.

1. Introduction

Chirality is a ubiquitous concept in chemistry with numerous chiral molecules such as glucids, amino acids, and the most famous elemental brick of life: DNA. Chirality was first revealed in crystals in 1848, when Louis Pasteur sorted out levogyre and dextrogyre ammonium tartrate crystals with a pair of tweezers under the microscope.[1] Chirality is also a key property in physics and especially in magnetism where an intense research effort has been recently devoted to chiral textures such as skyrmions, merons, and hopfions among many others.[2] These chiral objects are envisioned as the most stable and smallest magnetic objects achievable thanks to their topological protection: topology being a branch of mathematics that focuses on the properties of geometrical objects that are preserved under continuous deformation.[3] Recently, the concept of chirality has been extended to ferroelectric materials.[4–7] Chiral ferroelectric textures are indeed tremendously appealing because they can reach ultimate sizes, they harbor negative capacitance[8,9] and might be switchable with low-power electric fields. Nanometer-scale polar vortices[10] and skyrmions[11] have recently been observed in oxide PbTiO₃/SrTiO₃ superlattices, triggered by a subtle interplay between electrical and elastic boundary conditions at interfaces. In such superlattices, polar chirality was revealed using resonant X-ray diffraction.[12] Topological defects were also reported in single ferroelectric layers[13–15] as well as in ferroelectric nanostructures.[16,17] Actually, ferroelectric chirality might be even more common than expected, emerging from simple ferroelectric domain walls when dipoles have to reorient between domains.[18] Ferroelectric domain walls are known to be tiny

S. Fusil, J. Fischer, P. Dufour, C. Carrétéro, V. Garcia
Unité Mixte de Physique CNRS
Thales
Université Paris-Saclay
Palaiseau 91767, France
E-mail: stephane.fusil@cnrs-thales.fr; vincent.garcia@cnrs-thales.fr
S. Fusil
Université d'Evry
Université Paris-Saclay
Evry 91000, France

J.-Y. Chauleau, M. Viret
SPEC
CEA
CNRS
Université Paris-Saclay
Gif-sur-Yvette 91191, France
X. Li, A. Gloter
Laboratoire de Physique des Solides
CNRS
Université Paris-Saclay
Orsay 91405, France
C. Léveillé, N. Jaouen
Synchrotron SOLEIL
Gif-sur-Yvette 91192, France

**ADVANCED
SCIENCE NEWS**
www.advancedsciencenews.com

**ADVANCED
ELECTRONIC
MATERIALS**
www.advelectronicmat.de

objects with only a few unit cells width, typically one order of magnitude smaller than their ferromagnetic counterpart. Nevertheless, their structure is nowadays considered very similar to the one observed in ferromagnets: numerous recent experimental observations suggest that they are not pure Ising-like but possess a Bloch or Néel component.[19–22]

Here, we report pristine chirality in a single epitaxial ferroelectric thin film, combining resonant elastic X-ray scattering and scanning transmission electron microscopy. Investigating "classical" striped-domain $BiFeO_3$ thin films grown on (110) orthorhombic scandate substrates,[23–28] we show that a net polar chirality emerges from a peculiar arrangement of domain walls. While the polarization evolves from one domain to another through the expected short path 71° domain wall, the following domain wall is no longer 71° but consists of a pair of 109° domain wall plus a hidden 71° domain wall. Interestingly, through both short and long paths, the polarization rotates in the easy plane imposed by the monoclinic distortion of the substrate. This domain wall sequence allows a full (360°) polarization rotation, and the sequence repetition locks this rotation sense, therefore building polar chirality.

2. Results and Discussion

2.1. Polar Chirality Revealed with Resonant Elastic X-Ray Scattering

$BiFeO_3$ epitaxial thin films, with typical thicknesses in the 30–60 nm range, were grown by pulsed laser deposition on $DyScO_3$ and $GdScO_3$ (110) orthorhombic substrates using $SrRuO_3$ buffer oxide electrodes, as described elsewhere.[29] The (001) pseudo-cubic oxide heterostructure is fully strained in both cases with high structural quality attested by X-ray diffraction.[29] While the oxide electrode induces a preferential downward orientation of the ferroelectric polarization,[30] the monoclinic symmetry of the (110) scandate substrates favors only two ferroelastic variants of the ferroelectric, which results in a self-organized stripe-domain pattern with 71° domain walls (**Figure 1**).[24] The single direction of the stripes over the whole sample is imposed by the charge neutrality of the domain walls.

The striped-domain ferroelectric period is typically of the order of 200 ± 30 nm, as revealed by in-plane piezoresponse force microscopy (PFM) images (Figure 1a).

Taking advantage of the system periodicity, we investigated the properties of the ferroelectric domain structures using resonant elastic X-ray scattering (REXS). The scattering patterns at the oxygen K-edge (530 eV) are displayed in **Figure 2**a,e for $BiFeO_3$ thin films grown on $DyScO_3$[18] and $GdScO_3$, respectively. For both cases, these scattering patterns feature two pairs of spots, labeled "1" and "2," symmetric with respect to the specular spot. Real-space imaging using atomic force microscopy (AFM) allows to disentangle the two sources of periodicity. First, a purely surface-related periodicity is induced by the atomic steps mimicking those of the parent substrate and reproduced by the epitaxial layer-by-layer growth. In these $DyScO_3$ and $GdScO_3$ substrates, the direction of the miscut changes by 90° from one to the other (Figure 2c,g), corresponding to the spots labelled "1" in Figure 2a,e. The fast Fourier transform (FFT) patterns of the AFM images confirm the correspondence of the "1" spots in reciprocal space, with periodicities of 148 ± 20 nm (Figure 2c) and 137 ± 20 nm (Figure 2g), matching those obtained by REXS (164 ± 20 nm and 142 ± 20 nm in Figure 2a,e, respectively). We can then attribute the first pair of spots (labeled "1") to the periodic steps on the surface topography of the films. We now turn to the second pair of spots (labeled "2"). Here again, for both samples, the orientation as well as the spacing between the diffracted spots are matching when comparing REXS (218 ± 20 and 175 ± 20 nm in Figure 2a,e, respectively) and the FFT patterns from in-plane PFM phase images (225 ± 20 nm and 180 ± 20 nm in Figure 2d,h, respectively). The second pair of spots (labeled "2") is then attributed to the periodic ferroelectric domain structure.

REXS experiments were performed for both helicities of circularly polarized X-rays. Figure 2b,f display the circular dichroism patterns, i.e., the difference between left and right circularly polarized X-rays normalized by their sum. For both $BiFeO_3$ samples, while the periodic structural features ("1") show no circular dichroism, the spots corresponding to the periodic ferroelectric domains ("2") show a clear dichroic signal. This circular dichroism contrast inversion (blue and red spots
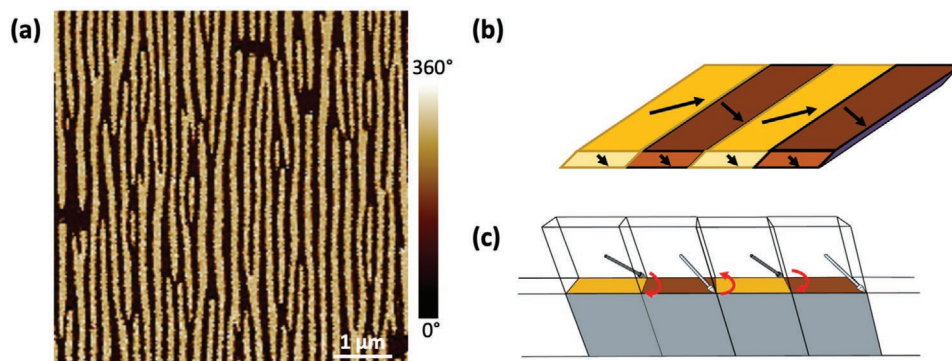
Figure 1. a) In-plane piezoresponse force microscopy phase image on a $BiFeO_3$ thin film grown on $DyScO_3$(110), illustrating the striped-domain pattern produced by two alternating ferroelastic domains. b) Sketch of the alternating ferroelectric domains with 71° domain walls. c) The monoclinic distortion of the substrate favors only two ferroelastic variants and the ferroelectric microstructure harbouring these two variants is sketched. The shortest path for polarization reorientation is represented by back and forth red arrows, giving rise to no net chirality.

ADVANCED
SCIENCE NEWS

www.advancedsciencenews.com

ADVANCED
ELECTRONIC
MATERIALS

www.advelectronicmat.de
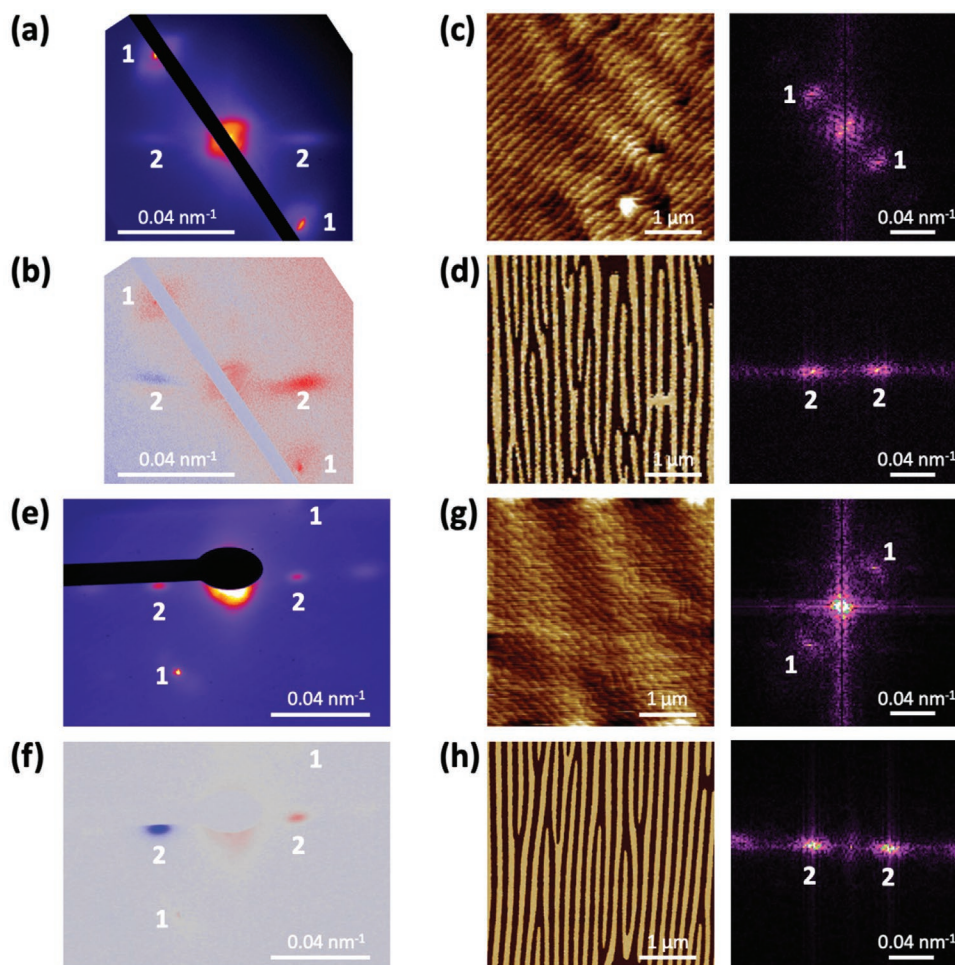
Figure 2. Periodic features in $BiFeO_3$ epitaxial thin films revealed by resonant elastic X-ray scattering and scanning probe microscopy. The $BiFeO_3$ thin films are grown on $DyScO_3(110)$ (a–d) and $GdScO_3(110)$ (e–h) substrates. a,e) Resonant elastic X-ray scattering patterns at the oxygen K-edge. b,f) Corresponding circular dichroic patterns. The vertical scales are −6% to +3% and −40% to +40% for (b) and (f), respectively. The data in (a) and (b) are adapted from ref. [18]. "1" and "2" spots stand for the topography and the ferroelectric periods, respectively. c,g) Unit-cell staircase surface of $BiFeO_3$ epitaxial films observed by atomic force microscopy. The vertical scales are 1 and 2 nm for (c) and (g), respectively. d,h) In-plane piezoresponse force microscopy phase images showing striped domain patterns with two ferroelastic variants. The vertical scales are 360° in (d) and (h). The fast Fourier transform (FFT) patterns are displayed on the right of each image in (c), (d), (g), and (h).

for +q and −q at the oxygen K-edge reveals the presence of a chiral polar order in the ferroelectric thin films.[31] As we expect the ferroelectric domains to be uniform with collinear polarization, the periodic chiral polar textures are likely to emerge from the ferroelectric domain walls of $BiFeO_3$. This implies that the domain walls are not Ising-like but possess a Bloch or Néel-like character with the polarization rotating always in the same sense. We note that this observation is valid for $BiFeO_3$ thin films grown on $DyScO_3$ and $GdScO_3$ substrates, imposing compressive and tensile strain, respectively. This is contrary to the expected rotation of polarization along the back and forth 71° domain walls, where the shortest path (red arrows in Figure 1c) would imply an opposite sense of rotation between neighboring domain walls and hence no net chirality. As $BiFeO_3$ is also antiferromagnetic with a periodic spin cycloid, one could wonder if a magnetic periodic texture could emerge from the ferroelectric domain arrangement, thus at the same period. We can rule out any magnetic contribution from the datasets acquired at the

O-K edge where the magnetic signal is negligible, if not absent. Nevertheless, the spots associated to the antiferromagnetic cycloid can be observed at the Fe L edge.[18,29]

2.2. Complex Domain Wall Path using Scanning Transmission Electron Microscopy

In order to get more insights into the chiral domain walls present in striped-domain $BiFeO_3$ thin films, we performed scanning transmission electron microscopy (STEM) experiments on cross-section specimens. Using medium angle annular dark field (MA-ADF), we were able to identify the expected 71° domain walls (**Figure 3**a). This 71° domain wall appears as a faint contrast in MA-ADF with a tilted plane with respect the growth axis. These walls are difficult to detect as the projection of polarization, perpendicularly to the [100] zone axis, is equivalent between both domains, and MA-ADF turned out

**ADVANCED
SCIENCE NEWS**

www.advancedsciencenews.com

**ADVANCED
ELECTRONIC
MATERIALS**

www.advelectronicmat.de
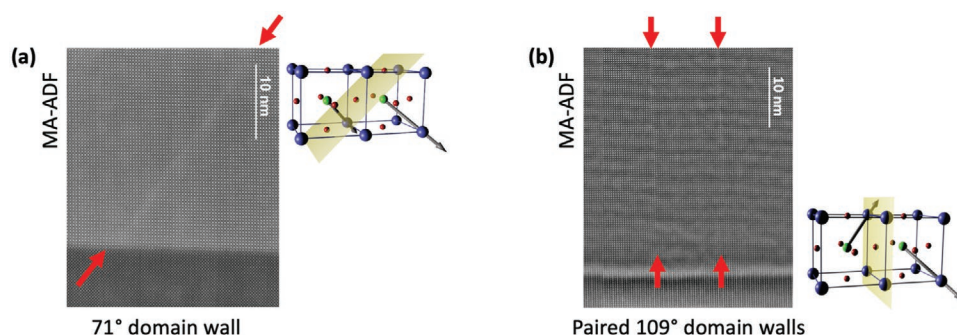
Figure 3. Medium angle annular dark field (MA-ADF) scanning transmission electron microscopy images of a) a 71° domain wall tilted away from the [001] growth axis and b) a pair of 109° vertical domain walls with a typical gap of 10 nm. The red arrows are guides to the eyes showing the locations of the domain walls. The 71° and 109° domain walls are sketched with the BiFeO$_3$ unit cell on the right of each panel.

to enhance their contrast as compared to more conventional high-angle annular dark field (HA-ADF). Surprisingly, pairs of vertical domain walls (Figure 3b) were also identified, typically separated by ≈10 nm. These can presumably be interpreted as 109° domain walls. Such observations imply that the ferroelectric landscape is much more complex than expected from PFM and X-ray diffraction characterizations.[29]

High-resolution HA-ADF images were also obtained in areas containing one or the other domain wall (**Figure 4**). Considering the different observations, we came up with the following scenario. The net polar chirality suggests that the periodic system alternates between a short path (domain 1 to domain 2, red boxed region in Figure 4), with a rotation of polarization in

a standard 71° domain wall (Figure 4a), and a long path (domain 2 to domain 1, blue boxed region in Figure 4), within a 10 nm area delimited by the two 109° domain walls (Figure 4b). From the relative displacements of the Fe atoms with respect to the barycenter of the Bi lattice, we were able to map the distribution of polarization across the domain walls.[19] One can clearly see that the polarization rotates continuously at the domain walls and its orientation is locally upward in the 10 nm gap defined by the two vertical walls. The polarization rotation, as projected on the plane perpendicular to the [100] zone axis, is fully compatible with a pair of 109° domain walls. To complete the long path of polar rotation from domain 2 to domain 1, we suggest that an additional 71° domain wall may be present in between
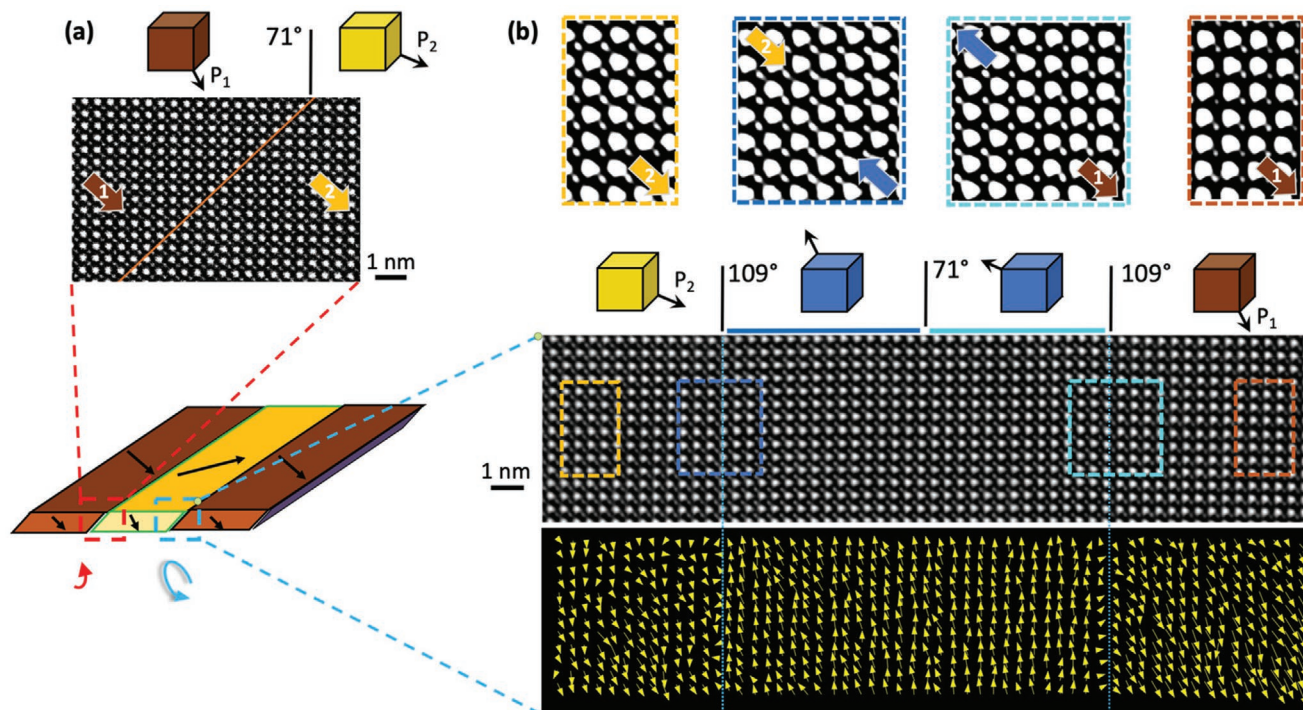
Figure 4. High-resolution high angle annular dark field (HA-ADF) images. a) A sketch of the striped domain structure of the BiFeO$_3$ thin film together with the HA-ADF image of the "simple" 71° domain wall (red box). b) The complex domain wall sequence (blue box in a) containing the pair of 109° domain walls. The middle panel shows an HA-ADF image of the area of interest together with sketches of the polar configurations. The top panel shows selected high-resolution HA-ADF images while the lower panel displays maps of polar displacements (in yellow) across this 10 nm area.

**ADVANCED
SCIENCE NEWS**

www.advancedsciencenews.com

**ADVANCED
ELECTRONIC
MATERIALS**

www.advelectronicmat.de
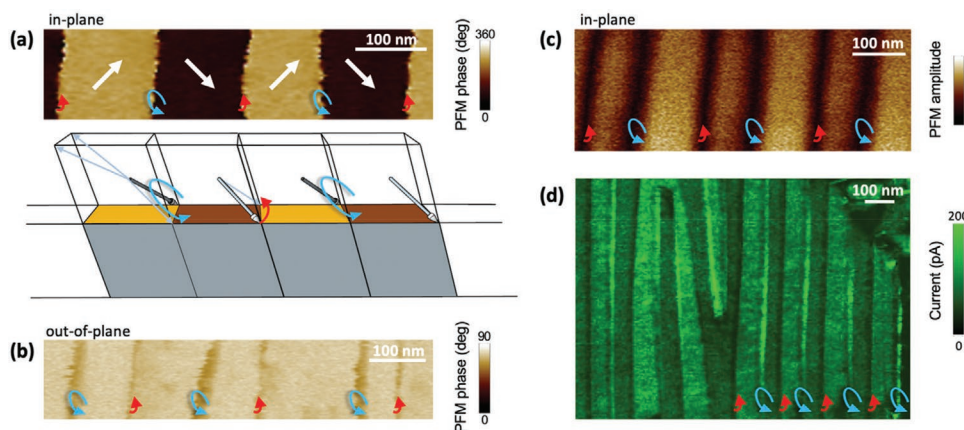
Figure 5. Scanning probe microscopy investigations of the $BiFeO_3$ domain walls. a) In-plane PFM phase image showing alternating striped domains. Sketch of the domains and the polar chirality involving short paths (red) and long paths (blue). b) Out-of-plane PFM phase image showing a small decrease of signal at the domain walls. Note that the vertical scale has been decreased to 90° to visualize this small phase contrast. c) In-plane PFM amplitude image showing a decreased signal at the domain walls. From (b) and (c), the width of every second domain wall is wider. d) Conductive atomic force microscopy map showing an enhanced conductivity at every second domain wall. The images in (a–d) were taken in different areas of the sample.

the 109° domain walls, but again hidden due to the [100] zone axis. We point out that all the ferroelectric variants being at play in this scenario are lying in the "easy" (110) plane, in which the polarization should be favored thanks to the monoclinic distortion arising from the substrate symmetry.

2.3. Scanning Probe Microscopy Insights into Chiral Windings

Given the small width (10 nm) of the long path area delimited by the pair of 109° domain walls, we are not able to resolve the local upward polarization orientation using PFM. By essence, PFM is not the most suitable approach to characterize domain walls as the PFM amplitude signal is decreased at their vicinity, and is even supposed to cancel at the border of two domains with out-of-phase responses. We are then unable to detect the upward polar nano-regions by PFM because of the resolution limitation in case of three domain walls stacked in a 10 nm width. This length scale even questions the standard definitions of domain walls in $BiFeO_3$ (namely 71°, 109°, and 180°) as each of these walls are a few unit cells wide so that we can consider the long path as a continuous domain wall with 289° (i.e., 109° + 71° + 109°) polarization rotation. Consequently, we looked more into the details of these ferroelectric domain walls using scanning probe microscopy. As displayed in **Figure 5**a, the high-resolution in-plane PFM phase image shows the two domains alternating and the chiral polar rotation at the domain walls is sketched below the image, as inferred from REXS and STEM observations. The red and blue arrows indicate the short and long paths, respectively. A careful look at the high-resolution out-of-plane PFM phase image (Figure 5b) reveals drops of signal associated to the ferroelectric domain walls. Interestingly, the width of these walls alternates between narrow and wider lines, possibly due to the short and long path, respectively. This is corroborated with the in-plane PFM amplitude (Figure 5c), which shows alternatively narrow and wider drops of signal, again possibly associated to the short and long

path domain walls, respectively. These scanning probe microscopy investigations support the fact that the system alternates between a simple 71° domain walls (short path) and a complex set of 109°/71°/109° domain walls (or 289° long path). Furthermore, conducting-AFM was performed applying a bias voltage of 1.7 V between the conducting AFM tip and the $SrRuO_3$ bottom electrode. Domain walls are clearly detected, defining the edges of the ferroelectric stripes seen by PFM. Their conduction remains weak and comparable to that of domains. Nevertheless, current maps indicate a different conduction between subsequent domain walls: one of them seems less conducting than the domains while the other appears as a double line with depressed and enhanced conductivities (Figure 5d). Notably, considering the domain wall sequences depicted in Figure 4, the "short path" 71° domain walls are neutral (Figure 4a), while the "long path" actually contains two charged 109° domain walls (Figure 4b), i.e., head to head and tail to tail for the left and right domain walls, respectively. Therefore, the enhanced or depressed conductions of the domain walls in Figure 5d could be related to their charged state.[17,33] However, these conducting-AFM currents maps do not allow us to conclude on the direct link between the complex domain wall sequences and their distinct conduction states, as these results are also reminiscent of those reported by Zhang et al.[32] on thick $BiFeO_3$ films grown by molecular beam epitaxy on $TbScO_3$ substrates, in which pure 71° domain walls showed enhanced conductions related to domain wall bending.

3. Conclusion

We show that the archetypical striped domain pattern in $BiFeO_3$ thin films displays an unexpected polar chirality emerging from ferroelectric domain walls. Resorting to resonant elastic X-ray scattering, we show that polar chirality is developed in striped-domains of $BiFeO_3$ thin films grown both under compressive or tensile strain. This is in contradiction

with the simple picture linking two different polarization domains by the shortest path available, giving no net chirality. Using scanning transmission electron microscopy, we reveal that there are actually two types of domain walls that coexist in the films: the simple short path alternates with a long path nanoregion schematized by three stacked domain walls. Despite the complexity of the domain wall sequence, the complete 360° polar rotation always occurs in the plane favored by the monoclinic distortion of the scandate substrates. The synergy between advanced real-space and reciprocal-space techniques allows to decipher how such a chiral winding proceeds. Nevertheless, the driving force for the emergence of polar chirality remains to be understood and further theoretical investigations are highly desirable.[34–36] From an experimental point of view, chirality may be extended to other ferroelectrics as this self-organized stripe domain landscape is common for standard ferroelectric thin films (as for example $BaTiO_3$ or $PbTiO_3$[15,37–40]).

4. Experimental Section

Sample Preparation and Characterization: The films are grown by pulsed laser deposition on $DyScO_3$(110) and $GdScO_3$(110) oxide single crystals using a KrF excimer laser (248 nm) with a laser fluence of 1 J cm^{-2}. Prior to the growth, the scandate substrates were annealed under oxygen flow for 3 h at 1000 °C. The $SrRuO_3$ bottom electrode was first grown at 660 °C under 0.2 mbar of oxygen pressure and with a laser frequency of 5 Hz. The $BiFeO_3$ thin films were subsequently grown at the same temperature under 0.36 mbar of oxygen pressure and a laser frequency of 2 Hz. After the growth, the samples were cooled down to room temperature under an oxygen pressure of 300 mbar. The thickness of the $BiFeO_3$ thin films was determined from X-ray reflectivity and double-checked from the Laue fringes of the 2θ-ω diffraction patterns. The thicknesses of the $BiFeO_3$ and $SrRuO_3$ layers grown on $GdScO_3$(110) (Figure 2e–h) are 56 and 5 nm, respectively. All the other experiments presented in the manuscript were performed on a $BiFeO_3$ (32 nm)/$SrRuO_3$ (10 nm)//$DyScO_3$(110) sample.

Resonant Elastic X-ray Scattering: Resonant elastic X-ray scattering (REXS) measurements were performed in reflectivity geometry at the O-K edge using the RESOXS diffractometer[41] at the SEXTANTS beamline[42] of SOLEIL synchrotron. The data were collected using nearly fully circular left and right X-ray polarizations delivered by the HU44 Apple2 undulator located at the I14-M straight section of the storage ring. REXS experiments were performed with the incoming X-rays at about 45° from the periodic stripes in Figure 2a,b while they were almost 90° from the periodic stripes in Figure 2e,f. These different azimuthal geometries explain the differences in the amplitude of the dichroic signals.

Scanning Transmission Electron Microscopy: Scanning transmission electron microscopy (STEM) experiments were performed using a Cs corrected Nion microscope operated at 100 keV. High angle annular dark field (HA-ADF) and medium angle annular dark field (MA-ADF) images were acquired with respectively 80–100 mrad and 40–80 mrad collection angle. The samples were prepared for STEM observation by gallium focus ion beam (FIB) where final surface polishing was done with a 2 keV ion beam.

Scanning Probe Microscopy: Piezoresponse force microscopy experiments were performed in a Nanoscope V, multimode (Bruker) using an external ac source (DS360, Stanford Research) to excite the $BiFeO_3$ thin film at a frequency of 35 kHz (far off resonance) with typical ac voltage excitations of 2 V peak to peak, and external lock-in amplifiers (SR830, Standford Research). In the high-resolution PFM experiments of Figure 5a–c, the pixel size is 2 nm. The conducting-AFM experiments were performed using a TUNA current amplifier. A voltage of 1.7 V was applied to the bottom electrode of $SrRuO_3$ while the tip was grounded during the current measurements of Figure 5d. We used super sharp diamond probes from Adama with a cantilever stiffness of 40 Nm^{-1} for both high-resolution PFM and conducting-AFM experiments.

Conflict of Interest

The authors declare no conflict of interest.

Data Availability Statement

The data that support the findings of this study are available from the corresponding author upon reasonable request.

[1] L. Pasteur, *Annal. Chim. Phys* **1848**, *24*, 442.
[2] B. Göbel, I. Mertig, O. A. Tretiakov, *Phys. Rep.* **2021**, *895*, 1.
[3] N. D. Mermin, *Rev. Mod. Phys.* **1979**, *51*, 591.
[4] J. Seidel, *Topological Structures in Ferroic Materials*, Springer, Cham, **2018**.
[5] J. Seidel, *Nat. Mater.* **2019**, *18*, 188.
[6] S. Das, Z. Hong, M. McCarter, P. Shafer, Y.-T. Shao, D. A. Muller, L. W. Martin, R. Ramesh, *APL Mater.* **2020**, *8*, 120902.
[7] G. Tian, W. D. Yang, X. S. Gao, J.-M. Liu, *APL Mater.* **2021**, *9*, 020907.
[8] P. Zubko, J. C. Wojdeł, M. Hadjimichael, S. Fernandez-Pena, A. Sené, I. Luk'yanchuk, J.-M. Triscone, J. Íñiguez, *Nature* **2016**, *534*, 524.
[9] A. K. Yadav, K. X. Nguyen, Z. Hong, P. García-Fernández, P. Aguado-Puente, C. T. Nelson, S. Das, B. Prasad, D. Kwon, S. Cheema, A. I. Khan, C. Hu, J. Íñiguez, J. Junquera, L.-Q. Chen, D. A. Muller, R. Ramesh, S. Salahuddin, *Nature* **2019**, *565*, 468.
[10] A. K. Yadav, C. T. Nelson, S. L. Hsu, Z. Hong, J. D. Clarkson, C. M. Schlepütz, A. R. Damodaran, P. Shafer, E. Arenholz, L. R. Dedon, D. Chen, A. Vishwanath, A. M. Minor, L. Q. Chen, J. F. Scott, L. W. Martin, R. Ramesh, *Nature* **2016**, *530*, 198.
[11] S. Das, Y. L. Tang, Z. Hong, M. A. P. Gonçalves, M. R. McCarter, C. Klewe, K. X. Nguyen, F. Gómez-Ortiz, P. Shafer, E. Arenholz, V. A. Stoica, S.-L. Hsu, B. Wang, C. Ophus, J. F. Liu, C. T. Nelson, S. Saremi, B. Prasad, A. B. Mei, D. G. Schlom, J. Íñiguez, P. García-Fernández, D. A. Muller, L. Q. Chen, J. Junquera, L. W. Martin, R. Ramesh, *Nature* **2019**, *568*, 368.
[12] P. Shafer, P. García-Fernández, P. Aguado-Puente, A. R. Damodaran, A. K. Yadav, C. T. Nelson, S.-L. Hsu, J. C. Wojdeł, J. Íñiguez,

**ADVANCED
SCIENCE NEWS**
www.advancedsciencenews.com

**ADVANCED
ELECTRONIC
MATERIALS**
www.advelectronicmat.de

L. W. Martin, E. Arenholz, J. Junquera, R. Ramesh, *Proc. Natl. Acad. Sci. USA* **2018**, *115*, 915.

[13] N. Balke, B. Winchester, W. Ren, Y. H. Chu, A. N. Morozovska, E. A. Eliseev, M. Huijben, R. K. Vasudevan, P. Maksymovych, J. Britson, S. Jesse, I. Kornev, R. Ramesh, L. Bellaiche, L. Q. Chen, S. V. Kalinin, *Nat. Phys.* **2012**, *8*, 81.

[14] Q. Zhang, L. Xie, G. Liu, S. Prokhorenko, Y. Nahas, X. Pan, L. Bellaiche, A. Gruverman, N. Valanoor, *Adv. Mater.* **2017**, *29*, 1702375.

[15] Y. Nahas, S. Prokhorenko, J. Fischer, B. Xu, C. Carrétéro, S. Prosandeev, M. Bibes, S. Fusil, B. Dkhil, V. Garcia, L. Bellaiche, *Nature* **2020**, *577*, 47.

[16] J. Ma, J. Ma, Q. Zhang, R. Peng, J. Wang, C. Liu, M. Wang, N. Li, M. Chen, X. Cheng, P. Gao, L. Gu, L.-Q. Chen, P. Yu, J. Zhang, C.-W. Nan, *Nat. Nanotech* **2018**, *13*, 947.

[17] W. Yang, G. Tian, Y. Zhang, F. Xue, D. Zheng, L. Zhang, Y. Wang, C. Chen, Z. Fan, Z. Hou, D. Chen, J. Gao, M. Zeng, M. Qin, L.-Q. Chen, X. Gao, J.-M. Liu, *Nat. Commun.* **2021**, *12*, 1306.

[18] J.-Y. Chauleau, T. Chirac, S. Fusil, V. Garcia, W. Akhtar, J. Tranchida, P. Thibaudeau, I. Gross, C. Blouzon, A. Finco, M. Bibes, B. Dkhil, D. D. Khalyavin, P. Manuel, V. Jacques, N. Jaouen, M. Viret, *Nat. Mater.* **2020**, *19*, 386.

[19] C. T. Nelson, B. Winchester, Y. Zhang, S.-J. Kim, A. Melville, C. Adamo, C. M. Folkman, S.-H. Baek, C.-B. Eom, D. G. Schlom, L.-Q. Chen, X. Pan, *Nano Lett.* **2011**, *11*, 828.

[20] L. Li, P. Gao, C. T. Nelson, J. R. Jokisaari, Y. Zhang, S.-J. Kim, A. Melville, C. Adamo, D. G. Schlom, X. Pan, *Nano Lett.* **2013**, *13*, 5218.

[21] S. Cherifi-Hertel, H. Bulou, R. Hertel, G. Taupier, K. D. Dorkenoo, C. Andreas, J. Guyonnet, I. Gaponenko, K. Gallo, P. Paruch, *Nat. Commun.* **2017**, *8*, 15768.

[22] Y. Zhang, H. Lu, L. Xie, X. Yan, T. R. Paudel, J. Kim, X. Cheng, H. Wang, C. Heikes, L. Li, M. Xu, D. G. Schlom, L.-Q. Chen, R. Wu, E. Y. Tsymbal, A. Gruverman, X. Pan, *Nat. Nanotech* **2018**, *13*, 1132.

[23] Y.-H. Chu, Q. He, C.-H. Yang, P. Yu, L. W. Martin, P. Shafer, R. Ramesh, *Nano Lett.* **2009**, *9*, 1726.

[24] Z. H. Chen, A. R. Damodaran, R. Xu, S. Lee, L. W. Martin, *Appl. Phys. Lett.* **2014**, *104*, 182908.

[25] D. Chen, Z. Chen, Q. He, J. D. Clarkson, C. R. Serrao, A. K. Yadav, M. E. Nowakowski, Z. Fan, L. You, X. Gao, D. Zeng, L. Chen, A. Y. Borisevich, S. Salahuddin, J.-M. Liu, J. Bokor, *Nano Lett.* **2017**, *17*, 486.

[26] S. Yang, R. Peng, Q. He, Y. Huang, Y. Huang, J. Yang, T. Chen, J. Guo, L. Chen, Y. Chu, C. Nan, P. Yu, *Ann. Phys.* **2018**, *530*, 1800130.

[27] D. Chen, D. Zhao, Z. Bai, J. Meng, X.-J. Ning, A. Jiang, *J. Appl. Phys.* **2018**, *123*, 044102.

[28] J. J. Steffes, R. A. Ristau, R. Ramesh, B. D. Huey, *Proc. Natl. Acad. Sci. USA* **2019**, *116*, 2413.

[29] A. Haykal, J. Fischer, W. Akhtar, J.-Y. Chauleau, D. Sando, A. Finco, F. Godel, Y. A. Birkhölzer, C. Carrétéro, N. Jaouen, M. Bibes, M. Viret, S. Fusil, V. Jacques, V. Garcia, *Nat. Commun.* **2020**, *11*, 1704.

[30] P. Yu, W. Luo, D. Yi, J. X. Zhang, M. D. Rossell, C.-H. Yang, L. You, G. Singh-Bhalla, S. Y. Yang, Q. He, Q. M. Ramasse, R. Erni, L. W. Martin, Y. H. Chu, S. T. Pantelides, S. J. Pennycook, R. Ramesh, *Proc. Natl. Acad. Sci. USA* **2012**, *109*, 9710.

[31] S. W. Lovesey, G. van der Laan, *Phys. Rev. B* **2018**, *98*, 155410.

[32] Y. Zhang, H. Lu, X. Yan, X. Cheng, L. Xie, T. Aoki, L. Li, C. Heikes, S. P. Lau, D. G. Schlom, L. Chen, A. Gruverman, X. Pan, *Adv. Mater.* **2019**, *31*, 1902099.

[33] A. Crassous, T. Sluka, A. K. Tagantsev, N. Setter, *Nat. Nanotech* **2015**, *10*, 614.

[34] K. C. Erb, J. Hlinka, *Phys. Rev. B* **2020**, *102*, 024110.

[35] H. J. Zhao, P. Chen, S. Prosandeev, S. Artyukhin, L. Bellaiche, *Nat. Mater.* **2021**, *20*, 341.

[36] A. N. Morozovska, R. Hertel, S. Cherifi-Hertel, V. Y. Reshetnyak, E. A. Eliseev, D. R. Evans, *Phys. Rev. B* **2021**, *104*, 054118.

[37] V. G. Koukhar, N. A. Pertsev, R. Waser, *Phys. Rev. B* **2001**, *64*, 214103.

[38] S. K. Streiffer, J. A. Eastman, D. D. Fong, C. Thompson, A. Munkholm, M. V. Ramana Murty, O. Auciello, G. R. Bai, G. B. Stephenson, *Phys. Rev. Lett.* **2002**, *89*, 067601.

[39] S. Matzen, O. Nesterov, G. Rispens, J. A. Heuver, M. Biegalski, H. M. Christen, B. Noheda, *Nat. Commun.* **2014**, *5*, 4415.

[40] A. S. Everhardt, S. Matzen, N. Domingo, G. Catalan, B. Noheda, *Adv. Electron. Mater.* **2016**, *2*, 1500214.

[41] N. Jaouen, J.-M. Tonnerre, G. Kapoujian, P. Taunier, J.-P. Roux, D. Raoux, F. Sirotti, *J. Synchrotron. Rad.* **2004**, *11*, 353.

[42] M. Sacchi, N. Jaouen, H. Popescu, R. Gaudemer, J. M. Tonnerre, S. G. Chiuzbaian, C. F. Hague, A. Delmotte, J. M. Dubuisson, G. Cauchon, B. Lagarde, F. Polack, *J. Phys.: Conf. Ser.* **2013**, *425*, 072018.